© 2023 IEEE. Personal use of this material is permitted. Permission from IEEE must be obtained for all other uses, in any current or future media, including reprinting/republishing this material for advertising or promotional purposes, creating new collective works, for resale or redistribution to servers or lists, or reuse of any copyrighted component of this work in other works.

Ergodic Performance Analysis of Reconfigurable Intelligent Surface Enabled Bidirectional NOMA

Ashish Rauniyar*, Olav N. Østerbø†, Jan Erik Håkegård*, Paal E. Engelstad‡
*Sustainable Communication Technologies, SINTEF Digital, Norway
†Telenor Research, Norway
‡Department of Technology Systems, University of Oslo, Norway
Email: (ashish.rauniyar, jan.e.hakegard)@sintef.no, olav.osterbo@getmail.no, paal.engelstad@its.uio.no

***Abstract*—This paper proposes and investigates a reconfigurable intelligent surface (RIS) enabled bidirectional non-orthogonal multiple access (NOMA) network termed as NOMA-RIS. Here, RIS allows multiple NOMA users in one group to communicate with or share information with multiple NOMA users in another group. Specifically, the two NOMA user groups send the data intended for exchange to the RIS. RIS reflects the NOMA signals allowing bidirectional communication between two NOMA user groups. In particular, under the Rician fading environment, we pay close attention to how well RIS-enabled bidirectional NOMA networks operate. Analytical expressions for tight upper bounds for the ergodic capacity are mathematically derived and verified with the simulation results. Comprehensive performance comparisons are presented, showing that our proposed bidirectional NOMA-RIS system can achieve enhanced capacity gains than RIS-enabled traditional orthogonal multiple access schemes. These comparisons also offer practical insights into the impact of various system parameters on the overall network performance.**

***Index Terms*—Bidirectional, reconfigurable intelligent surface, non-orthogonal multiple access (NOMA), ergodic capacity, rician fading.**

I. Introduction

The advent of reconfigurable intelligent surfaces (RISs) has caused a profound revolution in the realm of wireless communication. It emerges as a promising technology to meet the ever-growing demands of the forthcoming sixth-generation (6G) wireless communication networks [1], [2]. The RIS is a cost-effective device comprising numerous electromagnetic elements designed to reflect signals and enhance the communication environment by optimizing the network's signal-to-interference-plus-noise ratio (SINR) and realize the smart radio environment [3]. More precisely, each individual element within the RIS can be programmed and electronically controlled by the RIS controller to adjust its phase shift independently. This enables the RIS to strategically steer impinging waves towards a desired direction.

In contrast to conventional relaying and multi-antenna systems like massive multiple-input multiple-output (MIMO), RIS offer an advantage by eliminating the need for intricate decoding, encoding processes, and expensive radio frequency (RF) equipment chains [4]. Hence, RISs are considered a more cost-effective solution [5]. In addition, one of the main advantages of RIS is that it offers seamless integration into building interiors and the surfaces of large vehicles, requiring minimal or no modifications to existing equipment and device software. This streamlined integration greatly reduces the costs associated with enhancing performance aspects such as energy efficiency [6], connectivity, and coverage extension for next-generation wireless communication networks [7], [8].

In addition to RIS, non-orthogonal multiple access (NOMA), which facilitates massive Internet of Things (IoT) connectivity and boosts the spectrum efficiency of the communication networks, has been identified as a key candidate for 6G [9]. In contrast to orthogonal multiple access (OMA) methods like orthogonal frequency-division multiple access (OFDMA) and time-division multiple access (TDMA), NOMA adopts a distinctive approach to user separation. More precisely, power-domain NOMA allows multiple users to utilize the same orthogonal resources and employs superposition coding to concurrently transmit distinct signals to different users by assigning varying power levels. Subsequently, it utilizes successive interference cancellation (SIC) at the receiver side to separate and decode these signals [10], [11].

Recognizing the significant potential of both RIS and NOMA as pivotal candidates for the development of 6G networks, recent endeavors have sought to integrate RIS with NOMA to enhance spectral and energy efficiency. In a study conducted by Liu et al. [12], a comprehensive exploration of RIS-empowered NOMA networks was undertaken, encompassing investigations into information-theoretic capacity limits and optimal RIS deployment strategies, both in static and dynamic RIS configurations. To tackle the challenge of mitigating mutual user interference, Khaleel et al. [13] delved into a downlink NOMA solution that incorporates RIS partitioning, examining the ergodic rates and outage probabilities for all users. Cheng et al. [14] explored the utilization of RIS to enable interaction between cell-edge user devices (UD) and the base station (BS) in the context of both one-way transmission scenarios and downlink and uplink NOMA networks. Their analysis delved into the outage and ergodic capacities of the BS-RIS-UD link under Nakagami-m fading conditions, shedding light on the quantification of system performance. It is noteworthy that these studies primarily focused on scenarios involving one-way transmission, where information flows from the BS to the RIS and is subsequently relayed to user terminals.

The combination of RIS-enabled networks with bidirec-

Author accepted manuscript version of the publication in
2023 33rd International Telecommunication Networks and Applications Conference
Published version: https://doi.org/10.1109/ITNAC59571.2023.10368523

tional communication can further improve the spectral efficiency of 6G networks. As shown in previous studies [15], [16], certain approaches have effectively implemented bidirectional communication in RIS-enabled communication networks. In the study conducted by Wang et al. [15], they investigated a two-way relay system that benefited from the assistance of RIS. Their research centered around formulating a joint beamforming and RIS design problem with the aim of maximizing the minimum signal-to-noise ratio (SNR) while adhering to a transmit power constraint at the base station (BS). It's worth noting that their study did not incorporate NOMA techniques. In contrast, Liu et al. [16] delved into the performance evaluation of a two-way NOMA network that leveraged RIS assistance. Their research specifically focused on assessing approximated expressions for outage probability and ergodic capacity, effectively integrating the NOMA paradigm into their study for improved wireless communication performance. It is important to note that the authors considered a system model with a single-user scenario and conducted their evaluations under Rayleigh fading. However, modelling communication links in RIS-based systems using Rayleigh distributions is imprecise. This is because there are considerable losses in the non-line-of-sight (NLoS) components, and strong line-of-sight (LoS) components are present. It is important to remember that RIS is typically utilized as a reflector, where the LoS component tends to be dominant [17]. Therefore, in this paper, we investigate a RIS-enabled bidirectional NOMA network termed as NOMA-RIS under Rician fading environment. In this context, the RIS enables multiple users belonging to one NOMA group to establish communication or exchange information with multiple users from another NOMA group.

The major contributions of this paper can be outlined as follows.

- We propose NOMA-RIS, a bidirectional NOMA network using RIS in a Rician fading environment. NOMA-RIS enables multiple users in one NOMA group to communicate with multiple users in another group.
- Our research focuses on investigating the ergodic performance of the NOMA-RIS system. Specifically, we derive tight upper bounds for the achievable rates under Rician fading. Our results demonstrate a close match between these derived bounds and the simulation results, highlighting the accuracy of our analysis.
- We present a comprehensive performance analysis showcasing the superiority of our proposed bidirectional NOMA-RIS system. Our results demonstrate significant capacity gains compared to traditional OMA-enabled RIS schemes.

II. RIS-ENABLED BIDIRECTIONAL NOMA (NOMA-RIS)

A. NOMA-RIS Channel Model

We have examined a bidirectional NOMA-RIS system, illustrated in Fig. 1. This system comprises multiple NOMA users in two groups: S (with users $S_1, S_2, S_3, ..., S_N$) and D (with users $D_1, D_2, D_3, ..., D_N$). These groups communicate and share information exclusively through the RIS. Notably, the direct link between groups S and D is assumed to be absent due to severe shadowing or obstruction. Therefore, the RIS, equipped with M reflecting elements, serves as the sole medium for information exchange between the two groups.

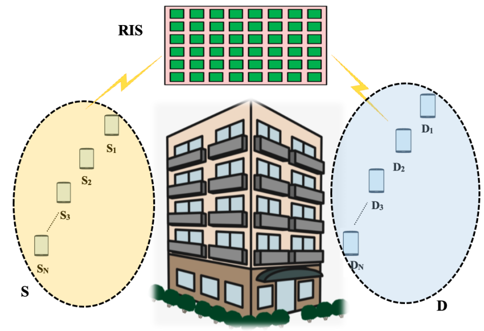

Fig. 1. Bidirectional NOMA-RIS system model.

In both groups S and D, each node operates as a full-duplex transceiver system with two antennas. Our assumptions align with those in a prior study by Liu et al. [16], where we also consider the availability of perfect channel status information (CSI) at the users. Specifically, we model the fading channel for the $S-RIS-D$ link as Rician. Additionally, we order the users within groups S and D based on their respective channel qualities, i.e. $|h_1|^2 > |h_2|^2 > |h_3|^2 > .....|h_N|^2$ in the group S and $|g_1|^2 < |g_2|^2 < |g_3|^2 < .....|g_N|^2$ in the group D. Here, $h_i = [h_1^1, h_2^2, \dots h_n^m \dots h_N^M]^H \in C^M$, $i \in 1, \dots N$ are denoted as channel coefficients of the links $S_1 \leftrightarrow RIS$, $S_2 \leftrightarrow RIS$, $\dots$, $S_n \leftrightarrow RIS$, $\dots$,$S_N \leftrightarrow RIS$, respectively, in group S, where $h_i^m = \sqrt{\alpha_i^m}(\sqrt{\frac{K}{K+1}} + \sqrt{\frac{1}{K+1}}\hat{h_i}^m)$, $\alpha_i = d_i^{-\alpha}$, d_i is the distance between i^{th} user in group S to RIS and α is the path-loss exponent, $\hat{h_i}^m \sim \mathcal{CN}(0,1)$, K is a Rician factor. Setting K to zero in the Rician fading channel results in a transformation to Rayleigh fading channels. On the other hand, as K approaches infinity, the channel predominantly consists of a fixed LoS component. Similarly, $g_j = [g_1^1$, g_2^2, $\dots g_n^m$ $\dots g_N^M]^H \in C^M$, $j \in 1, \dots N$ are denoted as channel coefficients of the links, $D_1 \leftrightarrow RIS$, $D_2 \leftrightarrow RIS$, $\dots$, $D_n \leftrightarrow RIS$, $\dots$,$D_N \leftrightarrow RIS$, respectively, in group D, where $g_j^m = \sqrt{\alpha_j^m}(\sqrt{\frac{K}{K+1}} + \sqrt{\frac{1}{K+1}}\hat{g_j}^m)$, $\alpha_j = d_j^{-\alpha}$, d_j is the distance between j^{th} user in group D to RIS and $\hat{g_j}^m \sim \mathcal{CN}(0,1)$. The effective cascade channel gains are represented as $h_i^H \Phi g_j$, where $\Phi = \text{diag}(\beta_1 e^{j\theta_1}, \cdots \beta_M e^{j\theta_M})$ forms an $M \times M$ diagonal phase-shifting matrix. In this matrix, the M main diagonal elements correspond to the reflecting elements of the RIS, where $\beta_m \in [0,1]$ and $\theta_m \in [0, 2\pi]$ denote the reflection coefficient and phase-shift for the m^{th} reflecting element, respectively.

B. NOMA-RIS System Model

To simplify our analysis without sacrificing generality, we consider a system model with $2N$ NOMA users distributed equally into two groups of N users each. Multiple pairs of users are formed within each group to create NOMA groups. Each NOMA group consists of users scheduled on the same channel, which is orthogonal to the channels used by the other group. In our NOMA-RIS system model, we designate the bandwidth for group S as $B_S = \tau B$ and for group D as $B_D = (1-\tau)B$, where B signifies the total available bandwidth in our system, with $0 < \tau \leq 1$. To ensure equitable bandwidth distribution, we evenly divide the total bandwidth B between group S and group D, resulting in $B_S = B_D = \frac{B}{2}$. This allocation approach adheres to the principle of proportional bandwidth fairness, as outlined in [18].

As per our system model, each NOMA user in group S, namely S_1 and S_2, and each user in group D, specifically D_1 and D_2, non-orthogonally transmit their information signals for exchange with the RIS. The signals transmitted by groups S and D at time t can be expressed as follows:

$$y_S(t) = \sqrt{a_1 P_T} h_1 x_{S_1} + \sqrt{a_2 P_T} h_2 x_{S_2}, \tag{1}$$

$$y_D(t) = \sqrt{b_1 P_T} g_1 x_{D_1} + \sqrt{b_2 P_T} g_2 x_{D_2}, \tag{2}$$

where P_T is the transmission power of the users in Group S and D, x_{S_1}, and x_{S_2} are the information signal of users S_1 and S_2 in Group S, and x_{D_1}, and x_{D_2} are the information signal of users D_1 and D_2 in Group D respectively. Also, a_1, and a_2 with $a_1 + a_2 = 1$ and $a_1 < a_2$, are the NOMA power allocation coefficients of S_1 and S_2 respectively, whereas b_1,and b_2 with $b_1 + b_2 = 1$ and $b_1 > b_2$, are the power allocation coefficients of D_1 and D_2, respectively.

The reflected signals received from RIS at Group S are given by:

$$y_S = h_i^H \Phi \left[\sqrt{b_1 P_T} g_1 x_{D_1} + \sqrt{b_2 P_T} g_2 x_{D_2} \right] + x_{I_S} + n_S \tag{3}$$

where x_{I_S} is the residual self-interfering signal with distribution $C\mathcal{N}(0, \sigma_{I_S}^2)$ and n_S is Additive White Gaussian Noise (AWGN) at group S with mean power $\sigma_{I_S}^2$.

Similarly, the reflected signals from RIS at Group D are given by:

$$y_D = g_i^H \Phi \left[\sqrt{a_1 P_T} h_1 x_{S_1} + \sqrt{a_2 P_T} h_2 x_{S_2} \right] + x_{I_D} + n_D \tag{4}$$

where x_{I_D} is the residual self-interfering signal with distribution $C\mathcal{N}(0, \sigma_{I_D}^2)$ and n_D is AWGN at group D with mean power $\sigma_{I_D}^2$.

C. Bidirectional NOMA-RIS Signals Decoding

Adhering to the NOMA principle, the received signal-to-interference-plus-noise ratio (SINR) values at users S_1 and S_2 within group S are expressed as:

$$\gamma_{S_1 \to D_2} = \frac{b_2 P_T |\sum_{i=1}^{M} \beta_i e^{j\theta_i} [h_1]^i [g_1]^i|^2}{b_1 P_T |\sum_{i=1}^{M} \beta_i e^{j\theta_i} [h_1]^i [g_1]^i|^2 + \sigma_{I_{S_1}}^2 + 1} \tag{5}$$

$$\gamma_{S_1 \to D_1} = \frac{b_1 P_T |\sum_{i=1}^{M} \beta_i e^{j\theta_i} [h_1]^i [g_1]^i|^2}{\sigma_{I_{S_1}}^2 + 1} \tag{6}$$

$$\gamma_{S_2 \to D_2} = \frac{b_2 P_T |\sum_{i=1}^{M} \beta_i e^{j\theta_i} [h_2]^i [g_2]^i|^2}{b_1 P_T |\sum_{i=1}^{M} \beta_i e^{j\theta_i} [h_2]^i [g_2]^i|^2 + \sigma_{I_{S_2}}^2 + 1} \tag{7}$$

Similarly, the received SINR values at users D_1 and D_2 in group D are given by:

$$\gamma_{D_2 \to S_1} = \frac{a_1 P_T |\sum_{i=1}^{M} \beta_i e^{j\theta_i} [g_2]^i [h_2]^i|^2}{a_2 P_T |\sum_{i=1}^{M} \beta_i e^{j\theta_i} [g_2]^i [h_2]^i|^2 + \sigma_{I_{D_2}}^2 + 1} \tag{8}$$

$$\gamma_{D_2 \to S_2} = \frac{a_2 P_T |\sum_{i=1}^{M} \beta_i e^{j\theta_i} [g_2]^i [h_2]^i|^2}{\sigma_{I_{D_2}}^2 + 1} \tag{9}$$

$$\gamma_{D_1 \to S_1} = \frac{a_1 P_T |\sum_{i=1}^{M} \beta_i e^{j\theta_i} [g_1]^i [h_1]^i|^2}{a_2 P_T |\sum_{i=1}^{M} \beta_i e^{j\theta_i} [g_1]^i [h_1]^i|^2 + \sigma_{I_{D_1}}^2 + 1} \tag{10}$$

III. Ergodic Performance Analysis of Bidirectional NOMA-RIS

A. Achievable Rate of S_1

The achievable rate of S_1 node associated with symbol x_{S_1} can be given as:

$$\begin{aligned} R_{S_1} &= E[\log_2(1 + \gamma_{S_1 \to D_1})] \\ &= E\left[\log_2 \left(1 + \frac{b_1 P_T |\sum_{i=1}^{M} \beta_i e^{j\theta_i} [h_1]^i [g_1]^i|^2}{\sigma_{I_{S_1}}^2 + 1} \right) \right] \end{aligned} \tag{11}$$

where E[·] denotes the statistical expectation operator.

B. Achievable Rate of S_2

The achievable rate of S_2 node associated with symbol x_{S_2} can be given as:

$$\begin{aligned} R_{S_2} &= E[\log_2 \left(1 + \min \left\{ \gamma_{S_1 \to D_2}, \gamma_{S_2 \to D_2} \right\} \right)] \\ &= E\Bigg[\log_2 \Bigg(1 + \min \Bigg\{ \frac{b_2 P_T |\sum_{i=1}^{M} \beta_i e^{j\theta_i} [h_1]^i [g_1]^i|^2}{b_1 P_T |\sum_{i=1}^{M} \beta_i e^{j\theta_i} [h_1]^i [g_1]^i|^2 + \sigma_{I_{S_1}}^2 + 1}, \\ &\qquad \frac{b_2 P_T |\sum_{i=1}^{M} \beta_i e^{j\theta_i} [h_2]^i [g_2]^i|^2}{b_1 P_T |\sum_{i=1}^{M} \beta_i e^{j\theta_i} [h_2]^i [g_2]^i|^2 + \sigma_{I_{S_2}}^2 + 1} \Bigg\} \Bigg) \Bigg] \end{aligned} \tag{12}$$

C. Achievable Rate of D_1

The achievable rate of D_1 node associated with symbol x_{D_1} can be given as:

$$\begin{aligned} R_{D_1} &= E[\log_2 \left(1 + \min \left\{ \gamma_{D_2 \to S_1}, \gamma_{D_1 \to S_1} \right\} \right)] \\ &= E\Bigg[\log_2 \Bigg(1 + \min \Bigg\{ \frac{a_1 P_T |\sum_{i=1}^{M} \beta_i e^{j\theta_i} [g_2]^i [h_2]^i|^2}{a_2 P_T |\sum_{i=1}^{M} \beta_i e^{j\theta_i} [g_2]^i [h_2]^i|^2 + \sigma_{I_{D_2}}^2 + 1}, \\ &\qquad \frac{a_1 P_T |\sum_{i=1}^{M} \beta_i e^{j\theta_i} [g_1]^i [h_1]^i|^2}{a_2 P_T |\sum_{i=1}^{M} \beta_i e^{j\theta_i} [g_1]^i [h_1]^i|^2 + \sigma_{I_{D_1}}^2 + 1} \Bigg\} \Bigg) \Bigg] \end{aligned} \tag{13}$$

D. Achievable Rate of D_2

The achievable rate of D_2 node associated with symbol x_{D_2} can be given as:

$$\begin{aligned} R_{D_2} &= E[\log_2(1+\gamma_{D_2\to S_2})] \\ &= E\left[\log_2\left(1+\frac{a_2 P_T|\sum_{i=1}^{M}\beta_i e^{j\theta_i}[g_2]^i[h_2]^i|^2}{\sigma^2_{I_{D_2}}+1}\right)\right] \end{aligned} \tag{14}$$

Theorem 1: Let $X \triangleq \sum_{i=1}^{M} U_i V_i$, where U_i and V_i are both Rician distributed with parameters k_1, $\Omega_1 = d_1^{-\alpha}$ and k_2, $\Omega_2 = d_2^{-\alpha}$ respectively. For Rician fading, the expected value of effective cascade channel gain $E[X^2]$ can be given as:

$$E[X^2] = M\Omega_1\Omega_2\left(1+\frac{(M-1)\pi^2}{16(k_1+1)(k_2+1)}\left(L_{\frac{1}{2}}(-k_1)L_{\frac{1}{2}}(-k_2)\right)^2\right) \tag{15}$$

where $L_{\frac{1}{2}}(.)$ is the Laguerre polynomial of order $\frac{1}{2}$, M is the total number of RIS elements.

proof: The probability density function (PDF) of a Rician distributed variable Z can be given as:

$$f_Z(x;k,\Omega) = \frac{2(k+1)x}{\Omega e^k} e^{-\frac{(k+1)}{\Omega}x^2} I_0\left(2x\sqrt{\frac{k(k+1)}{\Omega}}\right)$$

where $I_0(.)$ is the modified Bessel function of the first kind with order zero. The Rician random variable Z moments are found by using MATHEMATICA©.

$$E[Z^K] = \left(\sqrt{\frac{\Omega}{k+1}}\right)^K \Gamma(1+\frac{K}{2})L_{\frac{K}{2}}(-k)$$

where $\Gamma(.)$ is incomplete Gamma function.

Since $X_i = U_i V_i$ is the product of two independent Rician random variables, the moments can be found as:

$$\begin{aligned} E[X_i^K] &= E[(U_iV_i)^K] = E[U_i^K]E[V_i^K] \\ &= \left(\sqrt{\frac{\Omega_1}{k_1+1}\frac{\Omega_2}{k_2+1}}\right)^K \left(\Gamma(1+\frac{K}{2})\right)^2 L_{\frac{K}{2}}(-k_1)L_{\frac{K}{2}}(-k_2) \end{aligned}$$

Therefore,

$$\begin{aligned} E[X_i] &= \frac{\pi}{4}\sqrt{\frac{\Omega_1}{k_1+1}\frac{\Omega_2}{k_2+1}} L_{\frac{1}{2}}(-k_1)L_{\frac{1}{2}}(-k_2) \\ \sigma^2_{X_1} &= E[X_i^2] - (E[X_i])^2 \\ &= \Omega_1\Omega_2\left(1-\frac{\pi^2}{16(k_1+1)(k_2+1)}\left(L_{\frac{1}{2}}(-k_1)L_{\frac{1}{2}}(-k_2)\right)^2\right) \end{aligned}$$

Since, $X \triangleq \sum_{i=1}^{M} U_i V_i$, then the mean and variance are obtained by multiplying by M of the mean and variance for the individual variables X_i, and hence we have: $E[X] = ME[X_i]$ and $\sigma^2_X = M\sigma^2_{X_1}$.

Moreover, by applying the definition of the variance, we then also find the expectation of X^2 to be:

$E[X^2] = \sigma^2_X + (E[M])^2 = M\sigma^2_{X_1} + M^2(E[X_i])^2$

Now, inserting the mean and variance of X_i from above, we finally find $E[X^2]$ as in Eq. (15). ■.

TABLE I

SIMULATION PARAMETERS.

Parameter	Symbol	Values
Distance between S_1 and RIS	d_{S_1-R}	10 m
Distance between S_2 and RIS	d_{S_2-R}	40 m
Distance between RIS and D_1	d_{R-D_1}	40 m
Distance between RIS and D_2	d_{R-D_2}	10 m
Path Loss Exponent	α	2.5
Rician Factor	K	10, 2, 0
Reflection Coefficients	β_i	0.8
Power Allocation Factor for NOMA	a_1	0.2
Power Allocation Factor for NOMA	a_2	0.8
Power Allocation Factor for NOMA	b_1	0.8
Power Allocation Factor for NOMA	b_2	0.2

E. Tight Upper Bound for the Achievable Rate for Bidirectional NOMA-RIS

For ideal passive beamforming, we have $\beta_i = \beta$, $\forall i$. By setting up the optimal phase-shift matrix for each of the reflecting elements of RIS, the achievable rate of S_1 from Eq. (11) can be rewritten as:

$$\hat{R_{S_1}} = \frac{1}{\ln 2}E\left[\ln\left(1+\frac{b_1 P_T \beta^2 X^2}{\sigma^2_{I_{S_1}}+1}\right)\right] \tag{16}$$

where $X = \sum_{i=1}^{M}[h_1]^i[g_1]^i$.

Now, an upper bound of the achievable rate of S_1 is found using Jensen's inequality.

$$R^{Upper}_{S_1} = \frac{1}{\ln 2}E\left[\ln\left(1+\frac{b_1 P_T\beta^2 X^2}{\sigma^2_{I_{S_1}}+1}\right)\right] \le \frac{1}{\ln 2}\ln\left(1+\frac{b_1 P_T \beta^2 E[X^2]}{\sigma^2_{I_{S_1}}+1}\right) \tag{17}$$

Substituting the value of $E[X^2]$ as derived in Theorem 1, Eq. (15) above, we finally get the tight upper bound for the achievable rate of S_1.

By following similar steps, it is straightforward to derive the tight upper bounds for the achievable rates of S_2, D_1, and D_2. Combining these tight upper bounds for the achievable rates of S_1, S_2, D_1, and D_2 provides the tight upper bound for the achievable sum rate of the bidirectional NOMA-RIS system.

IV. RESULTS & DISCUSSION

In this section, we validate our analytically derived results for the ergodic capacity of the proposed NOMA-RIS system by comparing them with Monte-Carlo simulation results. The simulation experiments were conducted using MATLAB, averaging over 10^4 random realizations of Rician fading channels. $\sigma^2_{I_{S_1}}$, $\sigma^2_{I_{S_2}}$, $\sigma^2_{I_{D_1}}$, and $\sigma^2_{I_{D_2}}$ were set to 1. The phase of each link was randomly generated between 0 and 2π. Unless mentioned otherwise, the simulation parameters used for the experiments are provided in Table I. For comparison, we devised a bidirectional OMA-RIS system in which the data transmission and exchange of information occur in four-time slots.

In Fig. 2, and Fig. 3, we present the achievable rate of S_1 and S_2 as a function of the number of RIS reflecting elements. The plots are obtained for different transmit SNR values and varying Rician K factors. It should be noted

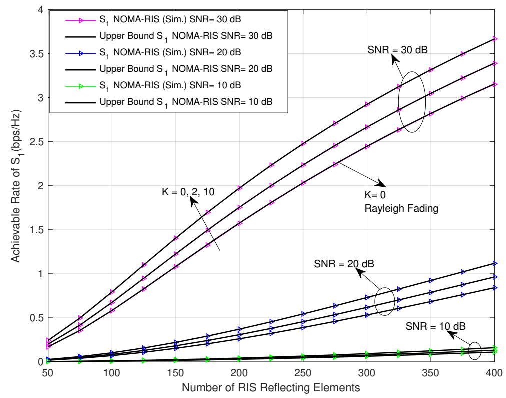

Fig. 2. Achievable rate of S_1.

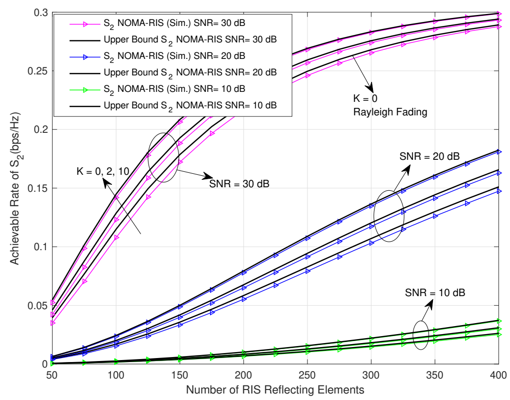

Fig. 3. Achievable rate of S_2.

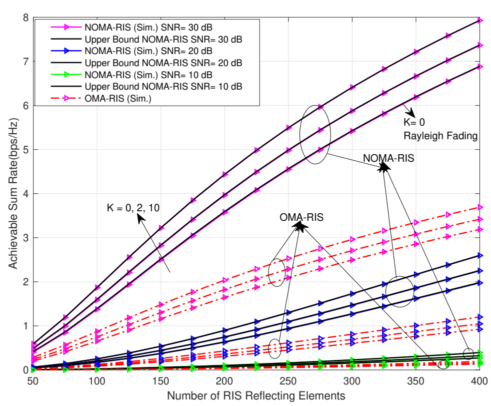

Fig. 4. Achievable sum rate of NOMA-RIS.

that the achievable rate performance for D_1 and D_2 is not shown since it is expected to be the same due to bidirectional communication. From Fig. 2 and Fig. 3, we observe that the achievable rate of S_1 is notably higher compared to S_2, and it increases with the number of RIS reflecting elements. These results align with our expectations. Additionally, the upper bounds derived in Section III closely match the simulation results, validating the accuracy of our analysis. Furthermore, we examine the achievable rate performance for S_1 and S_2 at higher transmit SNRs, such as 30 dB, and observe that the achievable rate increases with the Rician K factor value. It is worth noting that when $K = 0$, the system undergoes a transformation to Rayleigh fading channels, which represents the worst-case scenario for our NOMA-RIS system.

In Fig. 4, we compare the achievable sum rate of our proposed bidirectional NOMA-RIS system with the bidirectional OMA-RIS system. The results clearly demonstrate that our NOMA-RIS system outperforms the OMA-RIS system across all values of RIS reflecting elements. This significant difference in performance can be attributed to the fact that in OMA-RIS, the exchange of information occurs over four-time slots, while our NOMA-RIS system achieves the message exchange within a single time slot.

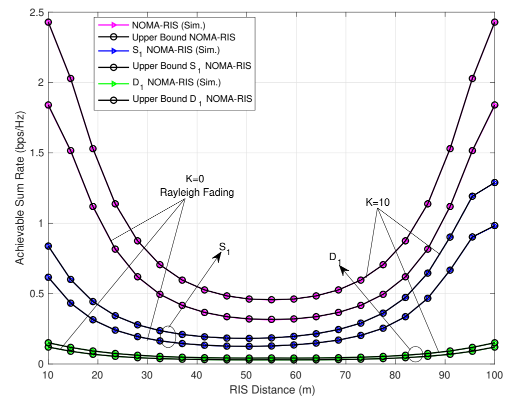

Fig. 5. Effect of RIS placement on the achievable sum rate of NOMA-RIS.

In Fig. 5, we investigate the impact of RIS placement on the achievable sum rate, considering different Rician K factors. The RIS location is varied between S_1 and D_1, ranging from 10 m to 100 m, with the constraint that the RIS is positioned at least 10 m above S_1 and D_1. From the results presented in Fig. 5, we observe that the achievable sum rate of the NOMA-RIS system is influenced by the proximity of the RIS to either S_1 or D_1. Specifically, the NOMA-RIS system achieves better performance when the RIS is positioned closer to either S_1 or D_1. Interestingly, minimal performance is achieved when the RIS is positioned equidistantly in the middle between S_1 and D_1. This behaviour can be explained by the far-field channel modelling of the NOMA-RIS system, where the path loss of the NOMA-RIS link is inversely proportional to the product of the distances of the incoming and outgoing channels.

In practical real-world scenarios, achieving ideal passive beamforming or continuous phase shifts can pose significant challenges and introduce complexity to the system. To address these challenges, the use of discrete phase shifts has emerged as a viable alternative. In this approach, each reflecting element of the RIS can only take on values from a predefined set of discrete phase-shift values, offering a more feasible implementation. However, it's crucial to account for the impact of imperfections in CSI on the performance of the NOMA-RIS system. In Fig 6, we investigate how discrete

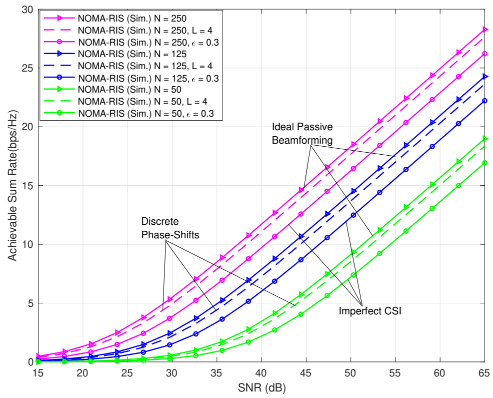

Fig. 6. Effect of discrete phase shifts ($L = 4$) and imperfect CSI ($\epsilon = 0.3$).

phase shifts and imperfect CSI affect the achievable sum rate of the bidirectional NOMA-RIS system. We specifically employ four uniformly quantized phase-shift levels ($L = 4$) and assume an imperfection level of $\epsilon = 0.3$ for the CSI. The results illustrate that both scenarios significantly impact the achievable sum rate, particularly at higher transmit signal-to-noise ratios (SNR) exceeding 25 dB. While increasing the number of RIS reflecting elements improves the achievable sum rate; it becomes evident that imperfect CSI has a more pronounced detrimental effect compared to discrete phase shifts. This highlights the crucial role of accurate CSI estimation in the NOMA-RIS system's performance. Imperfect CSI leads to inaccuracies in the phase-shift settings, resulting in a degradation of the achievable sum rate. As a result, careful consideration and improvement of CSI estimation techniques are essential to mitigate performance degradation in practical NOMA-RIS deployments.

V. Conclusions and Future Works

This paper focused on proposing and investigating a bidirectional NOMA-RIS system operating in a Rician fading environment. By leveraging the RIS, we enabled efficient bidirectional communication between two NOMA user groups. Through extensive simulations, we validated the performance of the proposed system by deriving tight upper bounds for the achievable rate and achievable sum rate. The results demonstrated the superiority of the bidirectional NOMA-RIS system over the benchmark bidirectional OMA-RIS approach in terms of achievable rate performance. Furthermore, we examined the impact of various factors on the performance of the bidirectional NOMA-RIS system. Our investigation revealed that RIS placement, discrete phase shift implementation, and imperfect CSI could potentially degrade the achievable rate performance. These findings emphasize the need for careful consideration and optimization of these factors in practical NOMA-RIS deployments.

In future, we will focus on studying the statistical characteristics of the RIS channel under various fading environments, allowing us to analyze metrics like outage probability and bit error rate and conduct comprehensive performance comparisons with relaying techniques. Additionally, we will explore the presence of direct links in the bidirectional NOMA-RIS system to further enhance its performance.

References

[1] S. Basharat, S. A. Hassan, H. Pervaiz, A. Mahmood, Z. Ding, and M. Gidlund, "Reconfigurable intelligent surfaces: Potentials, applications, and challenges for 6g wireless networks," *IEEE Wireless Communications*, vol. 28, no. 6, pp. 184–191, 2021.

[2] C. Pan, H. Ren, K. Wang, J. F. Kolb, M. Elkashlan, M. Chen, M. Di Renzo, Y. Hao, J. Wang, A. L. Swindlehurst *et al.*, "Reconfigurable intelligent surfaces for 6g systems: Principles, applications, and research directions," *IEEE Communications Magazine*, vol. 59, 2021.

[3] C. Huang, A. Zappone, G. C. Alexandropoulos, M. Debbah, and C. Yuen, "Reconfigurable intelligent surfaces for energy efficiency in wireless communication," *IEEE transactions on wireless communications*, vol. 18, no. 8, pp. 4157–4170, 2019.

[4] Z. Abdullah, G. Chen, S. Lambotharan, and J. A. Chambers, "A hybrid relay and intelligent reflecting surface network and its ergodic performance analysis," *IEEE Wireless Communications Letters*, vol. 9, no. 10, pp. 1653–1657, 2020.

[5] S. Basharat, S. A. Hassan, A. Mahmood, Z. Ding, and M. Gidlund, "Reconfigurable intelligent surface-assisted backscatter communication: A new frontier for enabling 6g iot networks," *IEEE Wireless Communications*, 2022.

[6] Q. Wu and R. Zhang, "Towards smart and reconfigurable environment: Intelligent reflecting surface aided wireless network," *IEEE communications magazine*, vol. 58, no. 1, pp. 106–112, 2019.

[7] Q. Li, M. Wen, S. Wang, G. C. Alexandropoulos, and Y.-C. Wu, "Space shift keying with reconfigurable intelligent surfaces: Phase configuration designs and performance analysis," *IEEE Open Journal of the Communications Society*, vol. 2, pp. 322–333, 2021.

[8] L. Dai, B. Wang, M. Wang, X. Yang, J. Tan, S. Bi, S. Xu, F. Yang, Z. Chen, M. Di Renzo *et al.*, "Reconfigurable intelligent surface-based wireless communications: Antenna design, prototyping, and experimental results," *IEEE access*, vol. 8, pp. 45 913–45 923, 2020.

[9] X. Mu, Z. Wang, and Y. Liu, "Noma for integrating sensing and communications towards 6g: A multiple access perspective," *IEEE Wireless Communications*, 2023.

[10] H. Sarieddeen, A. Abdallah, M. M. Mansour, M.-S. Alouini, and T. Y. Al-Naffouri, "Terahertz-band mimo-noma: Adaptive superposition coding and subspace detection," *IEEE Open Journal of the Communications Society*, vol. 2, pp. 2628–2644, 2021.

[11] A. Rauniyar, P. Engelstad, and O. N. Østerbø, "Rf energy harvesting and information transmission based on noma for wireless powered iot relay systems," *Sensors*, vol. 18, no. 10, p. 3254, 2018.

[12] Y. Liu, X. Mu, X. Liu, M. Di Renzo, Z. Ding, and R. Schober, "Reconfigurable intelligent surface-aided multi-user networks: Interplay between noma and ris," *IEEE Wireless Communications*, vol. 29, no. 2, pp. 169–176, 2022.

[13] A. Khaleel and E. Basar, "A novel noma solution with ris partitioning," *IEEE Journal of Selected Topics in Signal Processing*, vol. 16, no. 1, pp. 70–81, 2021.

[14] Y. Cheng, K. H. Li, Y. Liu, K. C. Teh, and H. V. Poor, "Downlink and uplink intelligent reflecting surface aided networks: Noma and oma," *IEEE Transactions on Wireless Communications*, vol. 20, no. 6, pp. 3988–4000, 2021.

[15] J. Wang, Y.-C. Liang, J. Joung, X. Yuan, and X. Wang, "Joint beamforming and reconfigurable intelligent surface design for two-way relay networks," *IEEE Transactions on Communications*, vol. 69, no. 8, pp. 5620–5633, 2021.

[16] Z. Liu, X. Yue, C. Zhang, Y. Liu, Y. Yao, Y. Wang, and Z. Ding, "Performance analysis of reconfigurable intelligent surface assisted two-way noma networks," *IEEE Transactions on Vehicular Technology*, vol. 71, no. 12, pp. 13 091–13 104, 2022.

[17] J. Xu and Y. Liu, "A novel physics-based channel model for reconfigurable intelligent surface-assisted multi-user communication systems," *IEEE Transactions on Wireless Communications*, vol. 21, no. 2, pp. 1183–1196, 2021.

[18] S. Qureshi, S. A. Hassan, and D. N. K. Jayakody, "Successive bandwidth division noma systems: Uplink power allocation with proportional fairness," in *2017 14th IEEE Annual Consumer Communications & Networking Conference (CCNC)*. IEEE, 2017, pp. 998–1003.